IEEE Access
Multidisciplinary : Rapid Review : Open Access Journal

Received September 22, 2021, accepted October 9, 2021, date of publication October 14, 2021, date of current version October 26, 2021.

Digital Object Identifier 10.1109/ACCESS.2021.3120205

An Improved Analytical Model of Magnetic Field in Surface-Mounted Permanent Magnet Synchronous Motor With Magnetic Pole Cutting

LIANLIAN GAO, ZHIQIANG CAI, YANPING LIANG, DONGMEI WANG, QUN NIU, AND JIA LI

School of Electrical and Electronic Engineering, Harbin University of Science and Technology, Harbin 150080, China

Corresponding author: Lianlian Gao (gaolianlian2018@163.com)

This work was supported in part by the Innovative Talent Project in Heilongjiang Province under Grant UNPYSCT-2020181, in part by the Postdoctoral Funding Project in Heilongjiang Province under Grant LBH-Z18101, and in part by the National Natural Science Foundation of China under Grant 51977053.

ABSTRACT This paper presents an analytical model for predicting the magnetic field performance of permanent magnet synchronous motor with permanent magnet cutting. In order to satisfy the boundary conditions, the defective permanent magnet is equivalent to a double-layer sector permanent magnet, and the size of the sector-shaped permanent magnet is determined, this process is obtained by an equivalent magnetic circuit model. Then, the motor is divided into four sub-domains: inner sector permanent magnet sub-domain, outer sector permanent magnet sub-domain, air gap sub-domain and stator slot sub-domain. Under the boundary conditions, the analytical solution and harmonic decomposition of the air gap magnetic flux density and cogging torque for several different permanent magnet cutting sizes under no-load condition are obtained by solving the Poisson equation and Laplace equation with the method of separating variables. The analytical model is verified by the finite element method. The results show that the error between the analytical method and the finite element method is less than 6%, and the solution time of the analytical method is only 0.59% of the finite element method, the chamfered structure proposed in the paper reduces the cogging torque amplitude 35%. Therefore, this method can provide powerful help for the initial design of permanent magnet motors.

INDEX TERMS Sub-domain model, cutting permanent magnet, magnetic circuit method, magnetic flux density.

I. INTRODUCTION

With the development of rare-earth permanent magnet (PM) materials, PM machines have attracted extensive attention by scholars. Compared with conventional machines, PM machines have the superiority in reliable operation, high efficiency, flexible shape and size. Therefore, PM machines are widely used in aerospace, electric vehicles, industrial production, agricultural production and other fields [1]–[5]. Designers pay close attention to the electromagnetic field distribution in PM machines, which is very important to design a PM machine with excellent performance.

The numerical method and analytical method are usually used in this field. The numerical method, represented by the finite element (FE) method, can better solve the non-linear phenomena and complex topology [6]. This method has universal applicability. However, in order to obtain accurate calculation results, it is necessary to divide the model with detailed mesh [7]. Inevitably, the FE method is quite time-consuming. The analytical method can provide physical insight to the motors, which usually analyzed from two directions: magnetic circuit model and magnetic field model. The magnetic circuit model establish the connection of magnetic flux, reluctance and magnetic potential by applying Kirchhoff's law according to the path of magnetic flux. The magnetic circuit model mainly adopts the equivalent magnetic network method and the equivalent magnetic circuit method [8]–[10]. However, these methods cannot analyze the harmonic characteristics of motor magnetic field. If we want to get more accurate results, we need to divide the magnetic

The associate editor coordinating the review of this manuscript and approving it for publication was Muhammad Zakarya.

circuit meticulously [11]. Therefore, this method is generally used in rough calculation of magnetic field. The magnetic field model mainly adopts the sub-domain method. This method divides the PM motor into several sub-domains, then obtains the Laplace equation or Poisson equation satisfied by the magnetic position function of each sub-domain. This process is derived from Maxwell's equations. Therefore, the core problem of this method is solving the differential equations. The definite solution condition is the boundary condition between the sub-domains [12]–[14]. The general solution of Fourier series can be obtained by using the separating variables method, and the result is very accurate [15], [16]. The difficulty of sub-domain method is establishing the special structure sub-domain model and deal with the nonlinear effect of magnetic circuit. In [17], [18], the auxiliary slot structure, iron core protruding structure in PM motor are treated respectively, and the FE method is used to verify. In [19]–[21], the equivalent current method and the equivalent air gap permeability method are used to solve the nonlinear effect of magnetic circuit. The results show that the improved method is more accurate. In addition, some magnetic field model can be implemented without solving the Laplace equation. For example, the magnetic island method [22], the air gap magnetic field modulation method [23], and the three-dimensional magnetic field calculation model based on the equivalent surface current of the permanent magnet [24].

In this paper, an improved analytical model for calculating the magnetic field distribution and cogging torque of PM motor is proposed. This method realizes the combination of magnetic circuit method and magnetic field method, which can be used surface-mounted PM motor with arbitrary angle cutting degree. The main work of this paper is as follows: In Section II, an improved analytical model is derived and obtained. Firstly, the angular PM is equivalent to two fan-shaped PMs, which is convenient to describe the magnetic field and matching boundary conditions of the PM. Then the air gap magnetic field distribution and cogging torque is obtained by solving the sub-domain differential equation. In Section III, the air gap flux density and cogging torque are calculated using the analytical model, and the accuracy of the algorithm is verified by the FE method. In Section IV, the advantages of the algorithm are discussed in terms of operation speed and accuracy. In Section V, we summarize the work of the paper and draw the final conclusion.

II. ANALYTICAL MODEL

The prototype model discussed in this paper is shown in Figure.1. In order to facilitate analysis, the following assumptions are made:

(1) PM keeps linear demagnetization state;
(2) core permeability is infinite;
(3) ignore end effect and iron core saturation effect.

The specific parameters of the motor are as follows: R_1 is the inner radius of PM; R_3 is the outer radius of PM; R_4 is the inner radius of stator; R_5 is the radius of the slot bottom; R_6 is the outer radius of stator.

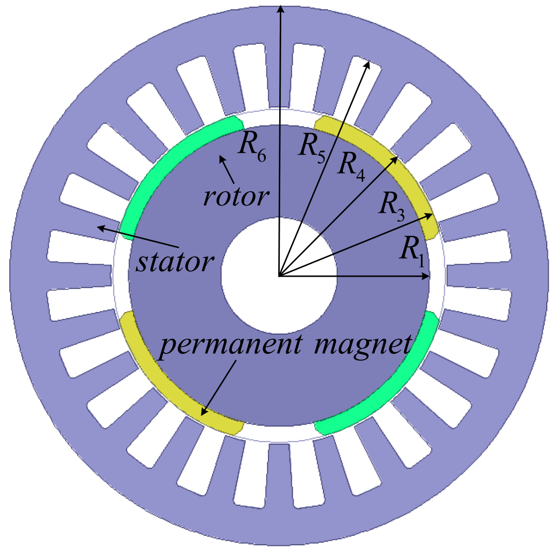

FIGURE 1. Model of surface mounted PM synchronous motor with pole clipping.

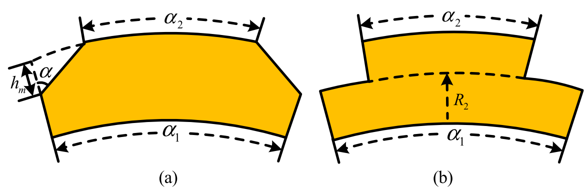

FIGURE 2. Equivalent of PM.

A. PM EQUIVALENT

In the classic sub-domain model, the boundary must be a standard arc [25], [26]. But the boundary of the contact air gap is no longer a standard arc when the corner of the PM is cut. Therefore, when establishing the sub-domain model, the boundary cannot be expressed by the standard boundary conditions, which will hinder solving the sub-domain differential equations. Therefore, the PM should be properly equivalent. In order to ensure the accuracy of the calculation results, the equivalent PM should not destroy the original distribution of the air gap magnetic field. Therefore, the defective PM is equivalent to a two-layer sector PM. According to the above principles, it is necessary to keep the polar arc angle between the PM and the rotor iron core boundary, the PM and the air gap boundary unchanged after equivalence [27], [28]. The schematic diagram of the PM equivalence is shown in the Figure.2. Where α_1 is the polar arc angle of the inner boundary of the PM, α_2 is the polar arc angle of the outer boundary of the PM, and R_2 is the inner diameter of the outer PM. It is worth noting that R_2 is an important quantity to be solved, and R_2 is solved by the magnetic circuit method, the solution process according to the principle of invariance of air gap magnetic field. Since the arc length difference between the inner and outer boundaries of the sector PM is very small, the PM is further simplified in the magnetic circuit method analysis process, as shown in Figure. 3. The equivalent magnetic circuit models of the pre and post

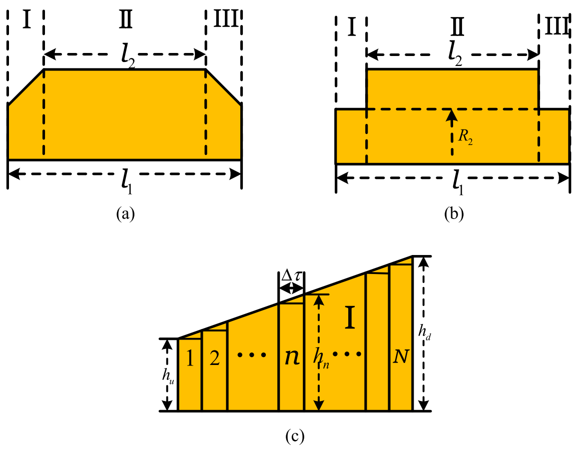

FIGURE 3. Further simplification of PM.

equivalent PMs are established respectively, as shown in Figure.4. The inner arc length l_1 of the PM and the outer arc length l_2 of the PM are derived as

$$l_1 = 0.5\,(R_1 + R_2)\,\alpha_1 \tag{1}$$
$$l_2 = 0.5\,(R_2 + R_3)\,\alpha_2 \tag{2}$$

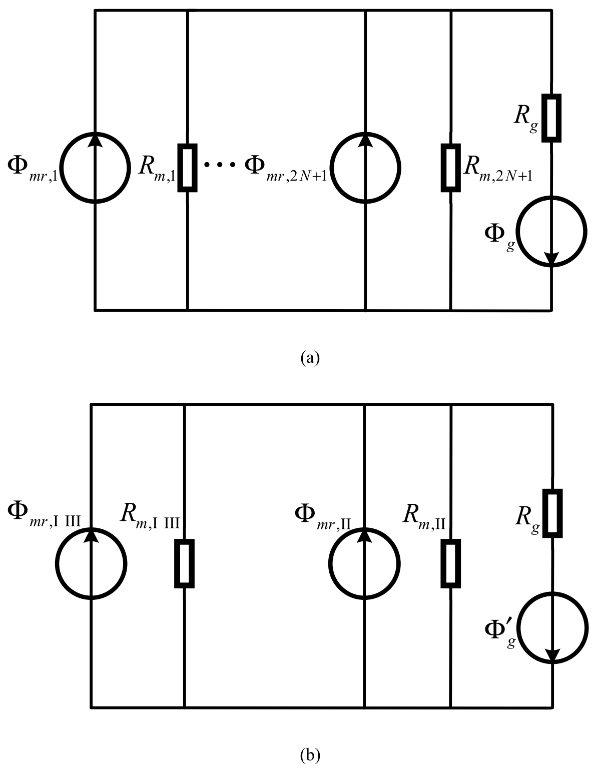

FIGURE 4. Equivalent magnetic circuit model of PM.

The defective PM is shown in the Figure.3(a), regions I and III of the model are two right angled trapezoids, and there is a big difference between the top and bottom. In order to better describe the magnetic resistance in this region, the infinitesimal method is used to divide regions I and III into N parts, as shown in the Figure.3(c), and the wide $\Delta\tau$ of the each PM is

$$\Delta\tau = \frac{l_1 - l_2}{2N} \tag{3}$$

In region I, the height h_n, magnetic resistance $R_{m,n}$ and magnetic flux $\Phi_{mr,n}$ of the nth PM are

$$h_n = h_u + \frac{(n-1)\,(h_d - h_u)}{N} \tag{4}$$
$$R_{m,n} = \frac{h_n}{\mu_0 \mu_r \Delta\tau L} \tag{5}$$
$$\Phi_{mr,n} = \Delta\tau L B_{mr} \tag{6}$$

where h_u and h_d are the length of the upper and lower bottom of the right-angled trapezoid, μ_0 is the permeability of vacuum, μ_r is the relative permeability of the PM, L is the axial length of the rotor, B_{mr} is the residual magnetic flux density of PM.

In region II, the height h_{N+1}, the magnetic resistance $R_{m,N+1}$ and magnetic flux $\Phi_{mr,N+1}$ of the $N+1$ th PM are

$$h_{N+1} = h_d \tag{7}$$
$$R_{m,N+1} = \frac{h_d}{\mu_0 \mu_r\,(l_1 - l_2)\,L} \tag{8}$$
$$\Phi_{mr,N+1} = (l_1 - l_2)\,L B_{mr} \tag{9}$$

In region III, the height h_{N+1+n}, the magnetic resistance $R_{m,N+1+n}$ and magnetic flux $\Phi_{mr,N+1}$ of the N + 1 + n th PM are

$$h_{N+1+n} = h_{N-n} \tag{10}$$
$$R_{m,N+1+n} = R_{m,N-n} \tag{11}$$
$$\Phi_{mr,N+1+n} = \Phi_{mr,N-n} \tag{12}$$

Ignoring the air gap between the poles, only the ring area between the PM and the stator iron core is considered as the effective air gap. According to the path taken by the magnetic flux, the average air gap magnetic resistance R_g corresponding to a single pole can be expressed as

$$R_g = \frac{R_4 - R_3}{\mu_0 \frac{R_3 + R_4}{2} \frac{\pi}{p} L} \tag{13}$$

where p is the number of pole pairs.

The equivalent magnetic circuit model of defective PM is shown in the Figure.4(a), which can be deduced according to Ohm's law of magnetic circuit

$$\Phi_{g,n} = \Phi_{mr,n} - \frac{\Phi_g R_g}{R_{m,n}}, \quad n = 1, \ldots, 2N+1 \tag{14}$$

Taking the sum of all the terms at both ends of equation (14) and further simplify

$$\Phi_g = \frac{\sum_{n=1}^{2N+1} \Phi_{mr,n}}{\left(1 + \sum_{n=1}^{2N+1} \frac{R_g}{R_{m,n}}\right)} \tag{15}$$

The Figure.3(b) shows the PM after equivalent, and the magnetic resistance $R_{m,\mathrm{I\,III}}$ and magnetic flux $\Phi_{mr,\mathrm{I\,III}}$ in the region I, III are

$$R_{m,\mathrm{I\,III}} = \frac{R_2 - R_1}{0.5\mu_0\mu_r L\left(R_1 + R_2\right)\left(\alpha_1 - \alpha_2\right)} \tag{16}$$

$$\Phi_{mr,\mathrm{I\,III}} = 0.5\left(R_1 + R_2\right)\left(\alpha_1 - \alpha_2\right) L B_{mr} \tag{17}$$

The magnet resistance $R_{m,\mathrm{II}}$ and magnetic flux $\Phi_{mr,\mathrm{II}}$ in the region II are

$$R_{m,\mathrm{II}} = \frac{R_3 - R_1}{0.5\mu_0\mu_r L\left(R_1 + R_3\right)\alpha_2} \tag{18}$$

$$\Phi_{mr,\mathrm{II}} = 0.5\left(R_1 + R_3\right)\alpha_2 L B_{mr} \tag{19}$$

The equivalent magnetic circuit of the PM after equivalent is shown in the Figure.4(b), which equivalent air gap flux can be deduced according to Ohm's law of magnetic circuit

$$\Phi'_g = \frac{\Phi_{mr,\mathrm{I\,III}} + \Phi_{mr,\mathrm{II}}}{\left(1 + \frac{R_g}{R_{m,\mathrm{I\,III}}} + \frac{R_g}{R_{m,\mathrm{II}}}\right)} \tag{20}$$

According to the principle that the air gap magnetic field is invariable, it can be obtained by substituting Φ_g for Φ'_g into equation (20)

$$\begin{aligned}\Gamma &= \frac{2\left(\Phi_{mr,\mathrm{I\,III}} + \Phi_{mr,\mathrm{II}} - \Phi_g\right)}{\mu_0\mu_r\Phi_g R_g L} \\ &= \left[\frac{\left(R_1 + R_2\right)\left(\alpha_1 - \alpha_2\right)}{R_2 - R_1} + \frac{\left(R_1 + R_3\right)\alpha_2}{R_3 - R_1}\right]\end{aligned} \tag{21}$$

where Γ is the new defined amount to simplify of sub-sequent reasoning.

By sorting out formula (21), the quadratic equation with R_2 to be solved is obtained

$$\Gamma_A R_2^2 + \Gamma_B R_2 + \Gamma_C = 0 \tag{22}$$

where

$$\Gamma_A = \Gamma - \alpha_1 - \frac{2R_1\alpha_2}{R_3 - R_1} = \frac{2R_1}{R_2 - R_1}\left(\alpha_1 - \alpha_2\right) \tag{23}$$

$$\begin{aligned}\Gamma_B &= -\left[\Gamma\left(R_1 + R_3\right) - \left(R_3 - R_1\right)\left(\alpha_1 - \alpha_2\right) - \alpha_2\frac{\left(R_1 + R_3\right)^2}{R_3 - R_1}\right] \\ &= \frac{-2\left(R_1R_3 + R_2R_1\right)}{R_2 - R_1}\left(\alpha_1 - \alpha_2\right)\end{aligned} \tag{24}$$

$$\begin{aligned}\Gamma_C &= 2R_1R_3\left[\Gamma - \frac{R_1\left(\alpha_1 - \alpha_2\right)}{R_2 - R_1} - \frac{\left(R_1 + R_3\right)\alpha_2}{R_3 - R_1}\right] \\ &= \frac{2R_1R_2R_3}{R_2 - R_1}\left(\alpha_1 - \alpha_2\right)\end{aligned} \tag{25}$$

The discriminant Δ of the equation can be expressed as

$$\Delta = \Gamma_B^2 - 4\Gamma_A\Gamma_C = \frac{4\left(R_1R_3 - R_1R_2\right)^2\left(\alpha_1 - \alpha_2\right)^2}{\left(R_2 - R_1\right)^2} > 0 \tag{26}$$

In practical sense, R_2 is the positive solution of the equation, which can be expressed as

$$R_2 = \frac{-\Gamma_B + \sqrt{\Gamma_B^2 - 4\Gamma_A\Gamma_C}}{2\Gamma_A} \tag{27}$$

According to the above reasoning, when R_2 is calculated according to equation (27), we think that the distribution of the original air gap magnetic field is not destroyed. This paper discusses the chamfering situation when $h_m = 1.75mm$, $\alpha = 45°$. Calculated by equation (27) $R_2 = 35.31mm$. The motor data required for the calculation process is provided in Table.1.

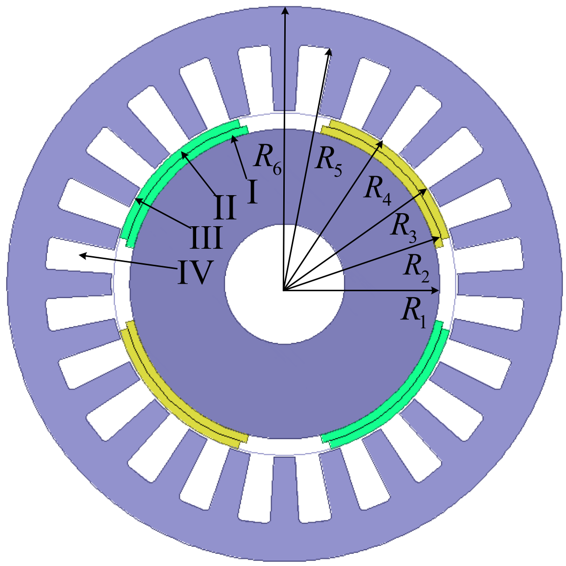

FIGURE 5. **The sub-domain model of PM synchronous motor after pole equivalence.**

B. SUB-DOMAIN MODEL

After equivalent treatment of PM, the solution model of the motor is finally determined, and the cross-section diagram is shown in Figure.5. The motor is divided into four sub-domains, namely inner PM sub-domain I, outer PM sub-domain II, air gap sub-domain III and stator open slot sub-domain IV. The partial differential equations of vector magnetic potential $\vec{A}$ in each sub-domain are derived from Maxwell's equation

$$\nabla^2\vec{A} = -\mu_0\mu_r\vec{J} - \mu_0\left(\nabla \times \vec{M}\right) \tag{28}$$

where $\vec{J}$ is current density, $\vec{M}$ is magnetization.

According to the difference of sub-domains, the differential equation of vector magnetic potential $\vec{A}$ of each sub-domain is simplified as

$$\nabla^2\vec{A}_{\mathrm{I}} = -\mu_0\left(\nabla \times \vec{M}_{\mathrm{I}}\right), \quad \text{in subdomain I} \tag{29}$$

$$\nabla^2\vec{A}_{\mathrm{II}} = -\mu_0\left(\nabla \times \vec{M}_{\mathrm{II}}\right), \quad \text{in subdomain II} \tag{30}$$

$$\nabla^2\vec{A}_{\mathrm{III}} = 0, \quad \text{in subdomain III} \tag{31}$$

$$\nabla^2\vec{A}_{\mathrm{IV}} = -\mu_0\mu_r\vec{J}_{\mathrm{IV}}, \quad \text{in subdomain IV} \tag{32}$$

Taking radial magnetization as an example, the radial magnetization M_{ir} and tangential magnetization $M_{i\theta}$ of the ith sub-domain can be expressed as [29]

$$\begin{cases} M_{ir} = \sum_{n/p=1,3,5\ldots}^{\infty} M_{ir,n} \cos\left[n\left(\theta - \theta_m\right)\right] \\ M_{i\theta} = \sum_{n/p=1,3,5\ldots}^{\infty} M_{i\theta,n} \sin\left[n\left(\theta - \theta_m\right)\right], \end{cases} \quad i = \mathrm{I}, \mathrm{II} \tag{33}$$

$$\begin{cases} M_{ir,n} = \frac{4pB_{mr}}{n\mu_0\pi} \sin\left(\frac{n\pi\alpha_{pi}}{2p}\right) \\ M_{i\theta,n} = 0, \end{cases} \quad i = \mathrm{I}, \mathrm{II} \tag{34}$$

where θ_m is the center position angle of N-pole of PM, α_{pi} is the pole arc coefficient of the PM in the i-th sub-domain.

In 2-D plane analysis, $\vec{B}$ has only tangential component and radial component, which leads to $\vec{A}$ having only z component

$$\vec{A}_{\mathrm{I}} = A_{\mathrm{I}}(r,\theta) \cdot \vec{e}_z, \quad \text{in subdomain I} \tag{35}$$

$$\vec{A}_{\mathrm{II}} = A_{\mathrm{II}}(r,\theta) \cdot \vec{e}_z, \quad \text{in subdomain II} \tag{36}$$

$$\vec{A}_{\mathrm{III}} = A_{\mathrm{III}}(r,\theta) \cdot \vec{e}_z, \quad \text{in subdomain III} \tag{37}$$

$$\vec{A}_{\mathrm{IV}} = A_{\mathrm{IV}}(r,\theta) \cdot \vec{e}_z, \quad \text{in subdomain IV} \tag{38}$$

In order to simplify the derivation process, two functions are defined [30]

$$P_z(x,y) = (x/y)^z + (y/x)^z \tag{39}$$

$$Q_z(x,y) = (x/y)^z - (y/x)^z \tag{40}$$

In the sub-domain I, $A_{\mathrm{I}}(r,\theta)$ satisfies the differential equation

$$\begin{cases} \frac{\partial^2 A_{\mathrm{I}}}{\partial r^2} + \frac{1}{r}\frac{\partial A_{\mathrm{I}}}{\partial r} + \frac{1}{r^2}\frac{\partial^2 A_{\mathrm{I}}}{\partial \theta^2} = \frac{\mu_0}{r}\frac{\partial M_{\mathrm{I}r}}{\partial \theta} \\ R_1 \le R \le R_2, \quad 0 \le \theta \le 2\pi \end{cases} \tag{41}$$

where $\vec{M}_{\mathrm{I}r}$ is the radial magnetization of the inner PM.

The boundary condition between PM and rotor iron core is satisfied

$$\left.\frac{\partial A_{\mathrm{I}}}{\partial r}\right|_{r=R_1} = 0 \tag{42}$$

The general solution of Poission equation is

$$A_{\mathrm{I}}(r,\theta) = \sum_{n=1}^{\infty} A_{\mathrm{I},n} \frac{P_n(r,R_1)}{P_n(R_2,R_1)} \cos(n\theta) + \sum_{n=1}^{\infty} C_{\mathrm{I},n} \frac{P_n(r,R_1)}{P_n(R_2,R_1)} \sin(n\theta) + \eta(r,\theta) \tag{43}$$

where $\eta(r,\theta)$ is the special solution of equation (41), it can be expressed as

$$\eta(r,\theta) = \sum_{n=1}^{\infty} X_n(r) \sin\left[n\left(\theta_m - \theta\right)\right] \tag{44}$$

where $X_n(r)$ can be expressed as

$$X_n(r) = \left[\frac{R_1}{n}\left(\frac{R_1}{r}\right)^n f_n'(R_1) + f_n'(r)\right] - \frac{P_n(r,R_1)}{P_n(R_2,R_1)}\left[\frac{R_1}{n}\left(\frac{R_1}{R_2}\right)^n f_n'(R_1) + f_n'(R_2)\right] \tag{45}$$

$$f_n(r) = \begin{cases} \frac{4B_r p}{\pi\left(1-n^2\right)} \cdot r \cdot \sin\left(\frac{n\pi}{2p}\alpha_{p1}\right), & n/p = 1,3,5\ldots \\ -\frac{2pB_r}{n\pi} \cdot r\ln r \cdot \sin\left(\frac{n\pi}{2p}\alpha_{p1}\right), & n = p = 1 \\ 0, & else \end{cases} \tag{46}$$

In the sub-domain II, $A_{\mathrm{II}}(r,\theta)$ satisfies the differential equation

$$\begin{cases} \frac{\partial^2 A_{\mathrm{II}}}{\partial r^2} + \frac{1}{r}\frac{\partial A_{\mathrm{II}}}{\partial r} + \frac{1}{r^2}\frac{\partial^2 A_{\mathrm{II}}}{\partial \theta^2} = \frac{\mu_0}{r}\frac{\partial M_{\mathrm{II}r}}{\partial \theta} \\ R_2 \le R \le R_3, \quad 0 \le \theta \le 2\pi \end{cases} \tag{47}$$

The general solution of Poission equation is

$$A_{\mathrm{II}}(r,\theta) = \sum_{n=1}^{\infty}\left(A_{\mathrm{II},n}\frac{R_2}{n}\frac{Q_n(r,R_3)}{P_n(R_2,R_3)} + B_{\mathrm{II},n}\frac{P_n(r,R_2)}{P_n(R_3,R_2)}\right) \times \cos(n\theta) + \sum_{n=1}^{\infty}\left(C_{\mathrm{II},n}\frac{R_2}{n}\frac{Q_n(r,R_3)}{P_n(R_2,R_3)} + D_{\mathrm{II},n}\frac{P_n(r,R_2)}{P_n(R_3,R_2)}\right) \times \sin(n\theta) + \xi(r,\theta) \tag{48}$$

where $\xi(r,\theta)$ is the special solution of equation (47), it can be expressed as

$$\xi(r,\theta) = \sum_{n=1}^{\infty} Y_n(r) \sin\left[n\left(\theta_m - \theta\right)\right] \tag{49}$$

$$Y_n(r) = \left[\frac{R_2}{n}\left(\frac{R_2}{r}\right)^n g_n'(R_2) + g_n'(r)\right] - \frac{P_n(r,R_2)}{P_n(R_3,R_2)}\left[\frac{R_2}{n}\left(\frac{R_2}{R_3}\right)^n g_n'(R_2) + g_n'(R_3)\right] \tag{50}$$

$$g_n(r) = \begin{cases} \frac{4B_r p}{\pi\left(1-n^2\right)} \cdot r \cdot \sin\left(\frac{n\pi}{2p}\alpha_{p2}\right), n/p = 1,3,5\ldots \\ -\frac{2pB_r}{n\pi} \cdot r\ln r \cdot \sin\left(\frac{n\pi}{2p}\alpha_{p2}\right), n = p = 1 \\ 0, else \end{cases} \tag{51}$$

In the sub-domain III, $A_{\mathrm{III}}(r,\theta)$ satisfies the differential equation

$$\begin{cases} \frac{\partial^2 A_{\mathrm{III}}}{\partial r^2} + \frac{1}{r}\frac{\partial A_{\mathrm{III}}}{\partial r} + \frac{1}{r^2}\frac{\partial^2 A_{\mathrm{III}}}{\partial \theta^2} = 0 \\ R_3 \le R \le R_4, \quad 0 \le \theta \le 2\pi \end{cases} \tag{52}$$

The general solution of Laplace equation is

$$\begin{aligned} & A_{\mathrm{III}}(r,\theta) \\ & = \sum_{n=1}^{\infty}\left[A_{\mathrm{III},n}\frac{R_3}{n}\frac{P_n(r,R_4)}{Q_n(R_3,R_4)}+B_{\mathrm{III},n}\frac{R_4}{n}\frac{P_n(r,R_3)}{Q_n(R_4,R_3)}\right] \\ & \quad\cdot\cos(n\theta)+\sum_{n=1}^{\infty}\left[C_{\mathrm{III},n}\frac{R_3}{n}\frac{P_n(r,R_4)}{Q_n(R_3,R_4)}\right. \\ & \quad\left.+D_{\mathrm{III},n}\frac{R_4}{n}\frac{P_n(r,R_3)}{Q_n(R_4,R_3)}\right]\sin(n\theta) \qquad (53) \end{aligned}$$

In the sub-domain IV, $A_{\mathrm{IV}}(r,\theta)$ satisfies the differential equation

$$\begin{cases} \dfrac{\partial^2 A_{\mathrm{IV}i}}{\partial r^2}+\dfrac{1}{r}\dfrac{\partial A_{\mathrm{IV}i}}{\partial r}+\dfrac{1}{r^2}\dfrac{\partial^2 A_{\mathrm{IV}i}}{\partial\theta^2}=-\mu_0 J_i \\ R_4\le R\le R_5, \quad \theta_i\le\theta\le\theta_i+\beta \end{cases} \qquad (54)$$

where J_i is the current density of i-th slot, θ_i is the initial position angle of i-th slot, and β is angle occupied by notch.

In this sub-domain, the contact boundary between the slot and the stator core meets the requirements

$$\left.\frac{\partial A_{\mathrm{IV},i}}{\partial r}\right|_{r=R_5}=0 \qquad (55)$$

$$\left.\frac{\partial A_{\mathrm{IV},i}}{\partial\theta}\right|_{\theta=\theta_i}=\left.\frac{\partial A_{\mathrm{IV},i}}{\partial\theta}\right|_{\theta=\theta_i+\beta}=0 \qquad (56)$$

The general solution of Poisson equation is simplified as

$$\begin{aligned} A_{\mathrm{IV},i}(r,\theta) &= \sum_{m=1}^{\infty}A_{\mathrm{IV},i,m}\frac{\beta R_4}{m\pi}\frac{P_{m\pi/\beta}(r,R_5)}{Q_{m\pi/\beta}(R_4,R_5)} \\ &\quad\cdot\cos\left(\frac{m\pi}{\beta}(\theta-\theta_i)\right)+\zeta(r,\theta) \qquad (57) \end{aligned}$$

where $\zeta(r,\theta)$ is the special solution of equation (54), it can be expressed as

$$\zeta(r,\theta)=A_{\mathrm{IV},i,0}+\frac{1}{2}\mu_0 J_i\left(R_5^2\ln r-\frac{1}{2}r^2\right) \qquad (58)$$

C. INTEGRAL COEFFICIENT

The general solution of the vector magnetic potential of each sub-domain is derived from the sub-domain model. The undetermined coefficients need to be solved by boundary conditions, which are the continuity of the vector magnetic potential and the continuity of the tangential magnetic field intensity.

At the interface of sub-domain I and sub-domain II, the boundary condition is

$$A_{\mathrm{I}}(R_2,\theta)=A_{\mathrm{II}}(R_2,\quad\theta),\ 0\le\theta\le 2\pi \qquad (59)$$

$$\left.\frac{\partial A_{\mathrm{I}}}{\partial r}\right|_{r=R_2}=\left.\frac{\partial A_{\mathrm{II}}}{\partial r}\right|_{r=R_2},\quad 0\le\theta\le 2\pi \qquad (60)$$

At the interface of sub-domain II and sub-domain III, the boundary condition is

$$A_{\mathrm{II}}(R_3,\theta)=A_{\mathrm{III}}(R_3,\theta),\quad 0\le\theta\le 2\pi \qquad (61)$$

$$\left.\frac{\partial A_{\mathrm{II}}}{\partial r}\right|_{r=R_3}=\left.\frac{\partial A_{\mathrm{III}}}{\partial r}\right|_{r=R_3},\quad 0\le\theta\le 2\pi \qquad (62)$$

At the interface of sub-domain III and sub-domain IV, the boundary condition is

$$A_{\mathrm{III}}(R_4,\theta)=A_{\mathrm{IV},i}(R_4,\theta),\ \theta_i\le\theta\le\theta_i+\beta \qquad (63)$$

$$\left.\frac{\partial A_{\mathrm{III}}}{\partial r}\right|_{r=R_4}=\left.\frac{\partial A_{\mathrm{IV},i}}{\partial r}\right|_{r=R_4},\quad \theta_i\le\theta\le\theta_i+\beta \qquad (64)$$

Combining with formula (43), (48), (59) we can get

$$\begin{aligned} A_{\mathrm{I},n} &= \frac{1}{\pi}\int_0^{2\pi}A_{\mathrm{II}}(R_2,\theta)\cos(n\theta)d\theta = A_{\mathrm{II},n}\frac{R_2}{n}\frac{Q_n(R_2,R_3)}{P_n(R_2,R_3)} \\ &\quad + B_{\mathrm{II},n}\frac{2}{P_n(R_3,R_2)}+Y_n(R_2)\sin(n\theta_m) \qquad (65) \end{aligned}$$

$$\begin{aligned} C_{\mathrm{I},n} &= \frac{1}{\pi}\int_0^{2\pi}A_{\mathrm{II}}(R_2,\theta)\sin(n\theta)d\theta = C_{\mathrm{II},n}\frac{R_2}{n}\frac{Q_n(R_2,R_3)}{P_n(R_2,R_3)} \\ &\quad + D_{\mathrm{II},n}\frac{2}{P_n(R_3,R_2)}+Y_n(R_2)\cos(n\theta_m) \qquad (66) \end{aligned}$$

Combining with formula (43), (48), (60) we can get

$$\begin{aligned} A_{\mathrm{II},n} &= \frac{1}{\pi}\int_0^{2\pi}\left.\frac{\partial A_{\mathrm{I}}}{\partial r}\right|_{r=R_2}\cos(n\theta)d\theta \\ &= A_{\mathrm{I},n}\frac{n}{R_2}\frac{Q_n(R_2,R_1)}{P_n(R_2,R_1)}+X_n'(R_2)\sin(n\theta_m) \qquad (67) \end{aligned}$$

$$\begin{aligned} C_{\mathrm{II},n} &= \frac{1}{\pi}\int_0^{2\pi}\left.\frac{\partial A_{\mathrm{I}}}{\partial r}\right|_{r=R_2}\sin(n\theta)d\theta \\ &= C_{\mathrm{I},n}\frac{n}{R_2}\frac{Q_n(R_2,R_1)}{P_n(R_2,R_1)}-X_n'(R_2)\cos(n\theta_m) \qquad (68) \end{aligned}$$

Combining with formula (48), (53), (61) we can get

$$\begin{aligned} B_{\mathrm{II},n} &= \frac{1}{\pi}\int_0^{2\pi}A_{\mathrm{III}}(R_3,\theta)\cos(n\theta)d\theta \\ &= A_{\mathrm{III},n}\frac{R_3}{n}\frac{P_n(R_3,R_4)}{Q_n(R_3,R_4)}+B_{\mathrm{III},n}\frac{R_4}{n}\frac{2}{Q_n(R_4,R_3)} \qquad (69) \end{aligned}$$

$$\begin{aligned} D_{\mathrm{II},n} &= \frac{1}{\pi}\int_0^{2\pi}A_{\mathrm{III}}(R_3,\theta)\sin(n\theta)d\theta \\ &= C_{\mathrm{III},n}\frac{R_3}{n}\frac{P_n(R_3,R_4)}{Q_n(R_3,R_4)}+D_{\mathrm{III},n}\frac{R_4}{n}\frac{2}{Q_n(R_4,R_3)} \qquad (70) \end{aligned}$$

Combining with formula (48), (53), (62) we can get

$$\begin{aligned} A_{\mathrm{III},n} &= \frac{1}{\pi}\int_0^{2\pi}\left.\frac{\partial A_{\mathrm{II}}}{\partial r}\right|_{r=R_3}\cos(n\theta)d\theta \\ &= A_{\mathrm{II},n}\frac{R_2}{R_3}\frac{2}{P_n(R_2,R_3)} \\ &\quad + B_{\mathrm{II},n}\frac{n}{R_3}\frac{Q_n(R_3,R_2)}{P_n(R_3,R_2)}+Y_n'(R_3)\sin(n\theta_m) \qquad (71) \end{aligned}$$

$$\begin{aligned} C_{\mathrm{III},n} &= \frac{1}{\pi}\int_0^{2\pi}\left.\frac{\partial A_{\mathrm{II}}}{\partial r}\right|_{r=R_3}\sin(n\theta)d\theta \\ &= C_{\mathrm{II},n}\frac{R_2}{R_3}\frac{2}{P_n(R_2,R_3)} \\ &\quad + D_{\mathrm{II},n}\frac{n}{R_3}\frac{Q_n(R_3,R_2)}{P_n(R_3,R_2)}+Y_n'(R_3)\cos(n\theta_m) \qquad (72) \end{aligned}$$

Combining with formula (53), (57), (63) we can get

$$A_{\mathrm{IV},i,0}+\frac{1}{2}\mu_0 J_i(R_5^2\ln R_4-\frac{1}{2}R_4^2)$$
$$=\frac{1}{\beta}\int_{\theta_i}^{\theta_i+\beta}A_{\mathrm{III}}(R_4,\theta)d\theta$$
$$=\sum_{n=1}^{\infty}\left[A_{\mathrm{III},n}\frac{2R_3}{n\beta}\frac{2}{Q_n(R_3,R_4)}+B_{\mathrm{III},n}\frac{2R_4}{n\beta}\frac{P_n(R_4,R_3)}{Q_n(R_4,R_3)}\right]\times M(n,i)$$
$$+\sum_{n=1}^{\infty}\left[C_{\mathrm{III},n}\frac{2R_3}{n\beta}\frac{2}{Q_n(R_3,R_4)}+D_{\mathrm{III},n}\frac{2R_4}{n\beta}\frac{P_n(R_4,R_3)}{Q_n(R_4,R_3)}\right]\times N(n,i) \tag{73}$$

$$A_{\mathrm{IV},i,m}\frac{\beta R_4}{m\pi}\frac{P_{m\pi/\beta}(R_4,R_5)}{Q_{m\pi/\beta}(R_4,R_5)}$$
$$=\frac{2}{\beta}\int_{\theta_i}^{\theta_i+\beta}A_{\mathrm{III}}(R_4,\theta)\cos\left(\frac{m\pi}{\beta}(\theta-\theta_i)\right)d\theta$$
$$=\sum_{n=1}^{\infty}\left[A_{\mathrm{III},n}\frac{2R_3}{n\beta}\frac{2}{Q_n(R_3,R_4)}+B_{\mathrm{III},n}\frac{2R_4}{n\beta}\frac{P_n(R_4,R_3)}{Q_n(R_4,R_3)}\right]\times F(m,n,i)$$
$$+\sum_{n=1}^{\infty}\left[C_{\mathrm{III},n}\frac{2R_3}{n\beta}\frac{2}{Q_n(R_3,R_4)}+D_{\mathrm{III},n}\frac{2R_4}{n\beta}\frac{P_n(R_4,R_3)}{Q_n(R_4,R_3)}\right]\times G(m,n,i) \tag{74}$$

Combining with formula (53), (57), (64) we can get

$$B_{\mathrm{III},n}=\frac{1}{\pi}\sum_{i=1}^{Q_s}\int_{\theta_i}^{\theta_i+\beta}\left.\frac{\partial A_{\mathrm{IV},i}}{\partial r}\right|_{r=R_4}\cos(n\theta)\,d\theta$$
$$=\sum_{i=1}^{Q_s}\frac{\mu_0 J_i}{2\pi}\left(\frac{R_5^2}{R_4}-R_4\right)M(n,i)+\sum_{i=1}^{Q_s}\sum_{m=1}^{\infty}\frac{A_{\mathrm{IV},m,i}}{\pi}F(m,n,i) \tag{75}$$

$$D_{\mathrm{III},n}=\frac{1}{\pi}\sum_{i=1}^{Q_s}\int_{\theta_i}^{\theta_i+\beta}\left.\frac{\partial A_{\mathrm{IV},i}}{\partial r}\right|_{r=R_4}\sin(n\theta)\,d\theta$$
$$=\sum_{i=1}^{Q_s}\frac{\mu_0 J_i}{2\pi}\left(\frac{R_5^2}{R_4}-R_4\right)N(n,i)+\sum_{i=1}^{Q_s}\sum_{m=1}^{\infty}\frac{A_{\mathrm{IV},m,i}}{\pi}G(m,n,i) \tag{76}$$

$$F(m,n,i)=\int_{\theta_i}^{\theta_i+\beta}\cos(n\theta)\cos\left[\frac{m\pi}{\beta}(\theta-\theta_i)\right]d\theta \tag{77}$$
$$G(m,n,i)=\int_{\theta_i}^{\theta_i+\beta}\sin(n\theta)\cos\left[\frac{m\pi}{\beta}(\theta-\theta_i)\right]d\theta \tag{78}$$
$$M(n,i)=\int_{\theta_i}^{\theta_i+\beta}\cos(n\theta)\,d\theta \tag{79}$$
$$N(n,i)=\int_{\theta_i}^{\theta_i+\beta}\sin(n\theta)\,d\theta \tag{80}$$

A linear system of equations with large order is obtained by simultaneous equations (65)-(76). The equations are written in matrix form

$$\mathbf{LX}=\mathbf{R} \tag{81}$$

where **L** is the coefficient matrix of the equations, **X** is the solution vector composed of undetermined coefficients in the general solution of the sub-domain equation, and **R** is the additional vector, which is usually the additional effect produced by the special solution of Poisson equation.

For the convenience of description, **L**, **X**, **R** is written in the form of block matrix, as shown in equation (82)-(84) at the bottom of the next page, where the submatrix I is the identity matrix, and the elements in the other submatrixs are given by equation (85)-(112).

$$I_{N\times N}=diag\,(1)_{N\times N} \tag{85}$$
$$L^{(1)}_{N\times N}=diag\left(-\frac{R_2}{n}\frac{Q_n(R_2,R_3)}{P_n(R_2,R_3)}\right)_N \tag{86}$$
$$L^{(2)}_{N\times N}=diag\left(-\frac{2}{P_n(R_3,R_2)}\right)_N \tag{87}$$
$$L^{(3)}_{N\times N}=diag\left(\frac{n}{R_2}\frac{Q_n(R_2,R_1)}{P_n(R_2,R_1)}\right)_N \tag{88}$$
$$L^{(4)}_{N\times N}=diag\left(-\frac{R_3}{n}\frac{P_n(R_3,R_4)}{Q_n(R_3,R_4)}\right)_N \tag{89}$$
$$L^{(5)}_{N\times N}=diag\left(-\frac{R_4}{n}\frac{2}{Q_n(R_4,R_3)}\right)_N \tag{90}$$
$$L^{(6)}_{N\times N}=diag\left(-\frac{R_2}{R_3}\frac{2}{P_n(R_2,R_3)}\right)_N \tag{91}$$
$$L^{(7)}_{N\times N}=diag\left(-\frac{n}{R_3}\frac{Q_n(R_3,R_2)}{P_n(R_3,R_2)}\right)_N \tag{92}$$
$$L^{(8)}_{N\times Q_sK}=\left(-\frac{F(k,n,q)}{\pi}\right)_{N\times Q_sK} \tag{93}$$
$$L^{(9)}_{N\times Q_sK}=\left(-\frac{G(k,n,q)}{\pi}\right)_{N\times Q_sK} \tag{94}$$
$$L^{(10)}_{Q_s\times N}=\left(-\frac{2R_3}{n\beta}\frac{M(n,q)}{Q_n(R_3,R_4)}\right)_{Q_s\times N} \tag{95}$$
$$L^{(11)}_{Q_s\times N}=\left(-\frac{R_4}{n\beta}\frac{P_n(R_4,R_3)\,M(n,q)}{Q_n(R_4,R_3)}\right)_{Q_s\times N} \tag{96}$$
$$L^{(12)}_{Q_s\times N}=\left(-\frac{2R_3}{n\beta}\frac{N(n,q)}{Q_n(R_3,R_4)}\right)_{Q_s\times N} \tag{97}$$
$$L^{(13)}_{Q_s\times N}=\left(-\frac{R_4}{n\beta}\frac{P_n(R_4,R_3)\,N(n,q)}{Q_n(R_4,R_3)}\right)_{Q_s\times N} \tag{98}$$
$$L^{(14)}_{Q_sK\times N}=\left(-\frac{4R_3}{n\beta}\frac{F(k,n,q)}{Q_n(R_3,R_4)}\right)_{Q_sK\times N} \tag{99}$$
$$L^{(15)}_{Q_sK\times N}=\left(-\frac{2R_4}{n\beta}\frac{P_n(R_4,R_3)\,F(k,n,q)}{Q_n(R_4,R_3)}\right)_{Q_sK\times N} \tag{100}$$
$$L^{(16)}_{Q_sK\times N}=\left(-\frac{4R_3}{n\beta}\frac{G(k,n,q)}{Q_n(R_3,R_4)}\right)_{Q_sK\times N} \tag{101}$$

$$L^{(17)}_{Q_sK\times N}=\left(-\frac{2R_4}{n\beta}\frac{P_n\left(R_4,R_3\right)G\left(k,n,q\right)}{Q_n\left(R_4,R_3\right)}\right)_{Q_sK\times N} \tag{102}$$

$$L^{(18)}_{Q_sK\times Q_sK}=diag\left(\frac{\beta R_4}{n\pi}\frac{P_{k\pi/\beta}\left(R_4,R_5\right)}{Q_{k\pi/\beta}\left(R_4,R_5\right)}\right)_{Q_sK} \tag{103}$$

$$R^{(1)}_{1\times N}=\left(Y_n\left(R_2\right)\sin\left(n\theta_m\right)\right)_{1\times N} \tag{104}$$

$$R^{(2)}_{1\times N}=\left(Y_n\left(R_2\right)\cos\left(n\theta_m\right)\right)_{1\times N} \tag{105}$$

$$R^{(3)}_{1\times N}=\left(-X'_n\left(R_2\right)\sin\left(n\theta_m\right)\right)_{1\times N} \tag{106}$$

$$R^{(4)}_{1\times N}=\left(X'_n\left(R_2\right)\cos\left(n\theta_m\right)\right)_{1\times N} \tag{107}$$

$$R^{(5)}_{1\times N}=\left(Y'_n\left(R_3\right)\sin\left(n\theta_m\right)\right)_{1\times N} \tag{108}$$

$$R^{(6)}_{1\times N}=\left(Y'_n\left(R_3\right)\cos\left(n\theta_m\right)\right)_{1\times N} \tag{109}$$

$$R^{(7)}_{1\times N}=\left(\sum_{q=1}^{Q_s}\frac{\mu_0 J_q}{2\pi}\left(\frac{R_5^2}{R_4}-R_4\right)M\left(n,q\right)\right)_{1\times N} \tag{110}$$

$$R^{(8)}_{1\times N}=\left(\sum_{q=1}^{Q_s}\frac{\mu_0 J_q}{2\pi}\left(\frac{R_5^2}{R_4}-R_4\right)N\left(n,q\right)\right)_{1\times N} \tag{111}$$

$$R^{(9)}_{1\times Q_s}=\left(-\frac{1}{2}\mu_0 J_q\left(R_5^2\ln R_4-\frac{1}{2}R_4^2\right)\right)_{1\times Q_s} \tag{112}$$

D. MAGNETIC FIELD CALCULATION

The integral coefficients of vector magnetic potential in each sub-domain are obtained by matrix equations(81), and the tangential and radial components of magnetic induction intensity in polar coordinates can be expressed as

$$B_r=\frac{1}{r}\frac{\partial A}{\partial\theta} \tag{113}$$

$$B_\theta=-\frac{\partial A}{\partial r} \tag{114}$$

Finally, the analytical expressions of radial and tangential air gap magnetic density are obtained

$$\begin{aligned}&B_{\mathrm{III}r}(R_{air},\theta)\\&=-\sum_{n=1}^{\infty}\left(A_{\mathrm{III},n}\frac{R_3}{R_{air}}\frac{P_n(R_{air},R_4)}{Q_n(R_3,R_4)}+B_{\mathrm{III},n}\frac{R_4}{R_{air}}\frac{P_n(R_{air},R_3)}{Q_n(R_4,R_3)}\right)\\&\quad\times\sin(n\theta)\\&\quad+\sum_{n=1}^{\infty}\left(C_{\mathrm{III},n}\frac{R_3}{R_{air}}\frac{P_n(R_{air},R_4)}{Q_n(R_3,R_4)}+D_{\mathrm{III},n}\frac{R_4}{R_{air}}\frac{P_n(R_{air},R_3)}{Q_n(R_4,R_3)}\right)\\&\quad\times\cos(n\theta)\end{aligned} \tag{115}$$

$$\begin{aligned}&B_{\mathrm{III}\theta}(R_{air},\theta)\\&=-\sum_{n=1}^{\infty}\left(A_{\mathrm{III},n}\frac{R_3}{R_{air}}\frac{Q_n(R_{air},R_4)}{Q_n(R_3,R_4)}+B_{\mathrm{III},n}\frac{R_4}{R_{air}}\frac{Q_n(R_{air},R_3)}{Q_n(R_4,R_3)}\right)\\&\quad\times\cos(n\theta)\\&\quad-\sum_{n=1}^{\infty}\left(C_{\mathrm{III},n}\frac{R_3}{R_{air}}\frac{Q_n(R_{air},R_4)}{Q_n(R_3,R_4)}+D_{\mathrm{III},n}\frac{R_4}{R_{air}}\frac{Q_n(R_{air},R_3)}{Q_n(R_4,R_3)}\right)\\&\quad\times\sin(n\theta)\end{aligned} \tag{116}$$

where R_{air} is the air gap radius, the value of R_{air} is the average of R_3 and R_4.

Using the Maxwell stress method, the cogging torque can be expressed as

$$T_{cog}=\frac{LR_{air}^2}{\mu_0}\int_0^{2\pi}B_{\mathrm{III}r}\left(R_{air},\theta\right)B_{\mathrm{III}\theta}\left(R_{air},\theta\right)d\theta \tag{117}$$

$$\mathbf{L}=\begin{pmatrix}
I_{N\times N} & 0 & L^{(1)}_{N\times N} & L^{(2)}_{N\times N} & 0 & 0 & 0 & 0 & 0 & 0 & 0 & 0\\
0 & I_{N\times N} & 0 & 0 & L^{(1)}_{N\times N} & L^{(2)}_{N\times N} & 0 & 0 & 0 & 0 & 0 & 0\\
L^{(3)}_{N\times N} & 0 & -I_{N\times N} & 0 & 0 & 0 & 0 & 0 & 0 & 0 & 0 & 0\\
0 & L^{(3)}_{N\times N} & 0 & 0 & -I_{N\times N} & 0 & 0 & 0 & 0 & 0 & 0 & 0\\
0 & 0 & 0 & I_{N\times N} & 0 & 0 & L^{(4)}_{N\times N} & L^{(5)}_{N\times N} & 0 & 0 & 0 & 0\\
0 & 0 & 0 & 0 & 0 & I_{N\times N} & 0 & 0 & L^{(4)}_{N\times N} & L^{(5)}_{N\times N} & 0 & 0\\
0 & 0 & L^{(6)}_{N\times N} & L^{(7)}_{N\times N} & 0 & 0 & I_{N\times N} & 0 & 0 & 0 & 0 & 0\\
0 & 0 & 0 & 0 & L^{(6)}_{N\times N} & L^{(7)}_{N\times N} & 0 & 0 & I_{N\times N} & 0 & 0 & 0\\
0 & 0 & 0 & 0 & 0 & 0 & 0 & I_{N\times N} & 0 & 0 & 0 & L^{(8)}_{N\times Q_sK}\\
0 & 0 & 0 & 0 & 0 & 0 & 0 & 0 & 0 & I_{N\times N} & 0 & L^{(9)}_{N\times Q_sK}\\
0 & 0 & 0 & 0 & 0 & 0 & L^{(10)}_{Q_s\times N} & L^{(11)}_{Q_s\times N} & L^{(12)}_{Q_s\times N} & L^{(13)}_{Q_s\times N} & I_{Q_s\times Q_s} & 0\\
0 & 0 & 0 & 0 & 0 & 0 & L^{(14)}_{Q_sK\times N} & L^{(15)}_{Q_sK\times N} & L^{(16)}_{Q_sK\times N} & L^{(17)}_{Q_sK\times N} & 0 & L^{(18)}_{Q_sK\times Q_sK}
\end{pmatrix} \tag{82}$$

$$\mathbf{X}=\begin{pmatrix}\left(A_{\mathrm{I},n}\right)_{1\times N},\left(C_{\mathrm{I},n}\right)_{1\times N},\left(A_{\mathrm{II},n}\right)_{1\times N},\left(C_{\mathrm{II},n}\right)_{1\times N},\left(B_{\mathrm{II},n}\right)_{1\times N},\left(D_{\mathrm{II},n}\right)_{1\times N},\\ \left(A_{\mathrm{III},n}\right)_{1\times N},\left(C_{\mathrm{III},n}\right)_{1\times N},\left(B_{\mathrm{III},n}\right)_{1\times N},\left(D_{\mathrm{III},n}\right)_{1\times N},\left(A_{\mathrm{IV},i,0}\right)_{1\times Q_s},\left(A_{\mathrm{IV},i,k}\right)_{1\times Q_sK}\end{pmatrix}^T \tag{83}$$

$$\mathbf{R}=\begin{pmatrix}R^{(1)}_{1\times N} & R^{(2)}_{1\times N} & R^{(3)}_{1\times N} & R^{(4)}_{1\times N} & (0)_{1\times N} & (0)_{1\times N} & R^{(5)}_{1\times N} & R^{(6)}_{1\times N} & R^{(7)}_{1\times N} & R^{(8)}_{1\times N} & R^{(9)}_{1\times Q_s} & (0)_{1\times Q_sK}\end{pmatrix}^T \tag{84}$$

TABLE 1. Units for magnetic properties main parameters of prototype machines.

Parameter	Quantity	Value
Outer radius of rotor(mm)	R_1	33.5
Outer diameter of permanent magnet(mm)	R_3	37
Stator inner diameter(mm)	R_4	37.5
Outer diameter of notch(mm)	R_5	50.914
Stator outer diameter(mm)	R_6	60
Rated speed(r/min)	N_1	1500
Number of stator slots(-)	Q_s	24
Number of pole pairs(-)	p	2
Rotor initial position angle(-)	θ_s	45°
Remanence density of permanent magnet(T)	B_r	1.1
Polar arc coefficient(-)	α_p	0.7
Notch angle(-)	β	8°

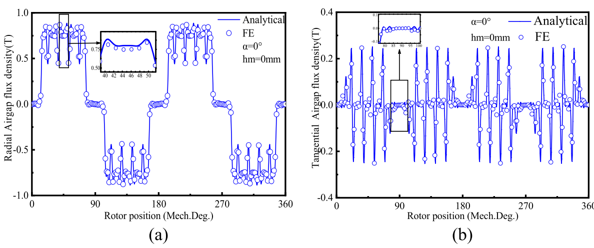

FIGURE 6. Air gap magnetic density without chamfering: (a) Radial component; (b) Tangential component.

So far, the analytical solution of the air gap flux density and the cogging torque considering the PM cutting is obtained. The algorithm will be verified in Section III.

III. ANALYTICAL CALCULATION AND FE VERIFICATION OF NO-LOAD MAGNETIC FIELD

Taking a 4-pole 24 slot surface mounted PM motor as an example, the air gap flux density are calculated by the proposed analytical method, and the analytical method is verified by two-dimensional FE method. The basic design parameters of the prototype are shown in Table.1. It should be noted that in the actual calculation of the general solution of the sub-domain equation, the harmonic number can only be taken to a finite degree, the parameter N is the maximum harmonic order of the vector magnetic potential in sub-domains I, II and III; the parameter K is the maximum harmonic order of the vector magnetic potential in the sub-domain IV. and the values calculated in this section are $N = 100$ and $K = 25$.

The calculation result of magnetic field distribution before chamfering is shown in the Figure.6. The results show that there are four inward concave spikes in the radial flux density waveform in each half cycle, which reveals that the slotting effect is the main reason for the distortion of the air gap magnetic field waveform of the PM motors, and each arc covered by the PM contains four slots, So the number of spines is four; The Figure.8 compares the distribution of air gap magnetic field when motor chamfering parameters

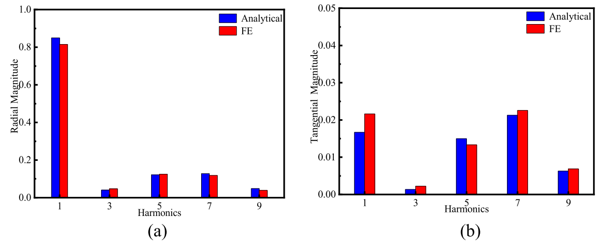

FIGURE 7. Harmonic decomposition of air gap magnetic density without chamfering: (a) Radial component; (b) Tangential component.

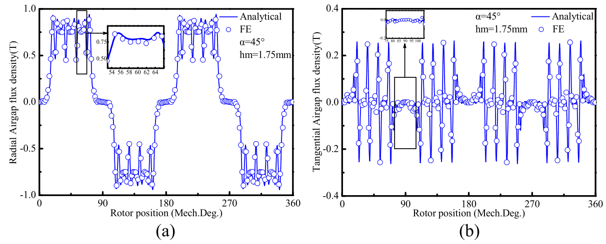

FIGURE 8. Air gap magnetic density with chamfering: (a) Radial component; (b) Tangential component.

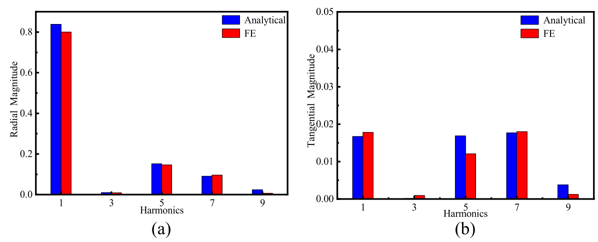

FIGURE 9. Harmonic decomposition of air gap magnetic density with chamfering: (a) Radial component; (b) Tangential component.

$\alpha = 45°$, $h_m = 1.75mm$. The results show that the radial air gap flux density after chamfering tends to bulge out at the edge of the PM, which is the influence of the PM chamfering on the air gap magnetic field; The analytical method is close to the FE method in both the fluctuation trend and the peak value. The Figure.7, Figure.9 are the harmonic decomposition graphs in two cases. Obviously, the harmonic components in two cases are also very consistent. On this basis, the Maxwell tensor method is used to calculate the cogging torque in two situations. The Figure.10 compares the results of the cogging torque obtained by the analytical method and the FE method. The cogging torque calculated by the proposed algorithm is very close to the FE method. In addition, the calculated peak cogging torque without chamfering is 745.5 mNm, and the peak cogging torque after chamfering is 438.4 mNm, which shows that the proposed permanent magnet chamfering structure can weaken the cogging torque effectively.

IV. DISCUSSION ON THE SPEED AND PRECISION OF ALGORITHM OPERATION

In the partial enlarged view of Figure.6 and Figure.8, it can be roughly seen from the visual effect that the analytical method is accurate, but the data that can reflect the error is often more convincing. In statistics, the root mean square (RMS) is usually used to compare the errors between data. But the value

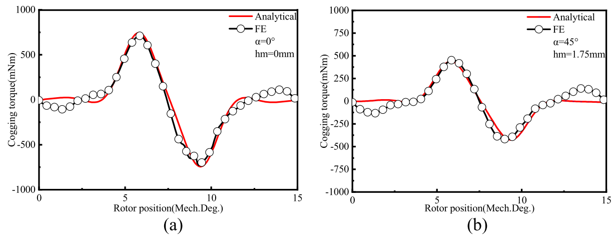

FIGURE 10. Cogging torque for diffierent conditions: (a) $\alpha = 0°$, $hm = 0mm$; (b) $\alpha = 45°$, $hm = 1.75mm$.

involved in the calculation is usually discrete. Therefore, the air gap magnetic density harmonics in several situations are decomposed, as shown in Figure.7 and Figure.9. The formula for calculating the RMS can be expressed as

$$RMS_{airgap} = \sqrt{\frac{\sum_i (m_A(i) - m_F(i))^2}{\sum_i m_F(i)^2}} \tag{118}$$

where $m_A(i)$ and $m_F(i)$ are the amplitude of the i-th harmonic air gap flux density respectively by analytical method and FE method.

TABLE 2. Error estimate of electromagnetic quantity.

Parameter	Quantity	RMS
$\alpha = 0°, h_m = 0mm$	$B_r(R_{air}, \theta)$	0.0242
	$B_\theta(R_{air}, \theta)$	0.1585
$\alpha = 45°, h_m = 1.75mm$	$B_r(R_{air}, \theta)$	0.0522
	$B_\theta(R_{air}, \theta)$	0.1998

The RMS in several situations is obtained from equation (118), as shown in Table.2. When $\alpha = 0°$, $h_m = 0mm$, the RMS of the radial air gap magnetic density is 0.0242, the RMS of the tangential air gap magnetic density is 0.1585; When $\alpha = 45°$, $h_m = 1.75mm$, the RMS the radial air gap magnetic density is 0.0522, the RMS of the magnetic density of the tangential air gap is 0.1998. Obviously, Data in the Table.2 can intuitively reflect that the error between the improved analytical method and the FE method is very small. This shows that the calculation accuracy of the analytical method is very high.

TABLE 3. Calculation time of analytical method and FE method.

Quantity	EFA	Analytical
Processor	Intel(R)Core(TM)i3-7100@3.9GHz	
Running memory	8.00GB	
Operating system	64bit Windows Operating System	
Computing time	845s	5s

On the other hand, the calculation speed of the algorithm can better reflect its application value, because the FE method is generally time-consuming. The two methods are respectively applied to two computers of the same model. The hardware properties of the computers and the calculation time of the two methods are shown in Table.3. The results show that the calculation speed of the analytical method is only 0.5917% of the FE method. In summary, the analytical method proposed in this article has excellent performance in terms of accuracy and speed.

V. CONCLUSION

This paper presents an improved analytical method for predicting the magnetic field performance of PM motor with PM cutting. This method realizes the combination of magnetic circuit method and magnetic field method. According to the same pole arc angle and the principle of magnetic field invariance, the defective PM is equivalent to a two-layer sector PM, which can better match the boundary conditions. In the equivalent analysis model, four sub-domains are established, and the Poisson equation or Laplace equation is solved by the method of separating variables. The FE results show that the method has high accuracy. In addition, the solution time of the analytical method is 5s, and that of the FE method is 845s, which shows that the analytical method has a huge advantage in terms of operating speed.

It is worth noting that it is assumed that the iron core is not saturated in this study, and the accuracy of the results is high. In spite of this, the high-precision and high-speed algorithm studied in this paper is still helpful to the motor designer, so the work in this paper is meaningful.

REFERENCES

[1] K. Li, A. Bouscayrol, S. Cui, and Y. Cheng, "A hybrid modular cascade machines system for electric vehicles using induction machine and permanent magnet synchronous machine," *IEEE Trans. Veh. Technol.*, vol. 70, no. 1, pp. 273–281, Jan. 2021.

[2] W. Li, G. Feng, C. Lai, Z. Li, J. Tian, and N. C. Kar, "Demagnetization analysis of interior permanent magnet machines under integrated charging operation," *IEEE Trans. Ind. Appl.*, vol. 55, no. 5, pp. 5204–5213, Sep. 2019.

[3] M. Wang, P. Zheng, C. Tong, Q. Zhao, and G. Qiao, "Research on a transverse-flux brushless double-rotor machine for hybrid electric vehicles," *IEEE Trans. Ind. Electron.*, vol. 66, no. 2, pp. 1032–1043, Feb. 2019.

[4] I. Boldea, L. N. Tutelea, L. Parsa, and D. Dorrell, "Automotive electric propulsion systems with reduced or no permanent magnets: An overview," *IEEE Trans. Ind. Electron.*, vol. 61, no. 10, pp. 5696–5711, Oct. 2014.

[5] A. Dadashnialehi, A. Bab-Hadiashar, Z. Cao, and A. Kapoor, "Intelligent sensorless antilock braking system for brushless in-wheel electric vehicles," *IEEE Trans. Ind. Electron.*, vol. 62, no. 3, pp. 1629–1638, Mar. 2015.

[6] A. Tessarolo, M. Mezzarobba, and R. Menis, "Modeling, analysis, and testing of a novel spoke-type interior permanent magnet motor with improved flux weakening capability," *IEEE Trans. Magn.*, vol. 51, no. 4, pp. 1–10, Apr. 2015.

[7] K. Yamazaki and H. Ishigami, "Rotor-shape optimization of interior-permanent-magnet motors to reduce harmonic iron losses," *IEEE Trans. Ind. Electron.*, vol. 57, no. 1, pp. 61–69, Jan. 2010.

[8] D. Cao, W. Zhao, J. Ji, L. Ding, and J. Zheng, "A generalized equivalent magnetic network modeling method for vehicular dual-permanent-magnet Vernier machines," *IEEE Trans. Energy Convers.*, vol. 34, no. 4, pp. 1950–1962, Dec. 2019.

[9] A. Hemeida, A. Lehikoinen, P. Rasilo, H. Vansompel, A. Belahcen, A. Arkkio, and P. Sergeant, "A simple and efficient quasi-3D magnetic equivalent circuit for surface axial flux permanent magnet synchronous machines," *IEEE Trans. Ind. Electron.*, vol. 66, no. 11, pp. 8318–8333, Nov. 2019.

[10] W. Tong, S. Wang, S. Dai, S. Wu, and R. Tang, "A quasi-three-dimensional magnetic equivalent circuit model of a double-sided axial flux permanent magnet machine considering local saturation," *IEEE Trans. Energy Convers.*, vol. 33, no. 4, pp. 2163–2173, Dec. 2018.

[11] J.-G. Lee, D.-K. Lim, and H.-K. Jung, "Analysis and design of interior permanent magnet synchronous motor using a sequential-stage magnetic equivalent circuit," *IEEE Trans. Magn.*, vol. 55, no. 10, pp. 1–4, Oct. 2019.

[12] S. T. Boroujeni and V. Zamani, "Influence of magnet shaping on cogging torque of surface-mounted PM machines," *Int. J. Numer. Model., Electron. Netw., Devices Fields*, vol. 29, no. 5, pp. 859–872, Sep. 2016.

[13] M. Hajdinjak and D. Miljavec, "Analytical calculation of the magnetic field distribution in slotless brushless machines with U-shaped interior permanent magnets," *IEEE Trans. Ind. Electron.*, vol. 67, no. 8, pp. 6721–6731, Aug. 2020.

[14] W. Tong, S. Li, X. Pan, S. Wu, and R. Tang, "Analytical model for cogging torque calculation in surface-mounted permanent magnet motors with rotor eccentricity and magnet defects," *IEEE Trans. Energy Convers.*, vol. 35, no. 4, pp. 2191–2200, Dec. 2020.

[15] Q. Lu, B. Wu, Y. Yao, Y. Shen, and Q. Jiang, "Analytical model of permanent magnet linear synchronous machines considering end effect and slotting effect," *IEEE Trans. Energy Convers.*, vol. 35, no. 1, pp. 139–148, Mar. 2020.

[16] W. Wang, M. Cheng, X. Li, M. Tong, and J. Qi, "Nonlinear analytical solution of magnetic field and performances of a spoke array Vernier permanent magnet machine," *IEEE Trans. Energy Convers.*, vol. 36, no. 1, pp. 173–185, Mar. 2021.

[17] Y. Oner, Z. Q. Zhu, L. J. Wu, X. Ge, H. L. Zhan, and J. T. Chen, "Analytical on-load subdomain field model of permanent-magnet Vernier machines," *IEEE Trans. Ind. Electron.*, vol. 63, no. 7, pp. 4105–4117, Jul. 2016.

[18] Z. Zhang, C. Xia, H. Wang, and T. Shi, "Analytical field calculation and analysis of surface inset permanent magnet machines with high saliency ratio," *IEEE Trans. Magn.*, vol. 52, no. 12, pp. 1–12, Dec. 2016.

[19] L. Wu, H. Yin, D. Wang, and Y. Fang, "A nonlinear subdomain and magnetic circuit hybrid model for open-circuit field prediction in surface-mounted PM machines," *IEEE Trans. Energy Convers.*, vol. 34, no. 3, pp. 1485–1495, Sep. 2019.

[20] L. Wu, H. Yin, D. Wang, and Y. Fang, "On-load field prediction in SPM machines by a subdomain and magnetic circuit hybrid model," *IEEE Trans. Ind. Electron.*, vol. 67, no. 9, pp. 7190–7201, Sep. 2020.

[21] P. Liang, F. Chai, Y. Yu, and L. Chen, "Analytical model of a spoke-type permanent magnet synchronous in-wheel motor with trapezoid magnet accounting for tooth saturation," *IEEE Trans. Ind. Electron.*, vol. 66, no. 2, pp. 1162–1171, Feb. 2019.

[22] M. M. Ghahfarokhi, A. D. Aliabad, S. T. Boroujeni, E. Amiri, and V. Z. Faradonbeh, "Analytical modelling and optimisation of line start LSPM synchronous motors," *IET Electr. Power Appl.*, vol. 14, no. 3, pp. 398–408, 2020.

[23] H. Zhang, W. Hua, D. Gerada, Z. Xu, and C. Gerada, "Analytical model of modular spoke-type permanent magnet machines for in-wheel traction applications," *IEEE Trans. Energy Convers.*, vol. 35, no. 3, pp. 1289–1300, Sep. 2020.

[24] R. Zhou, G. Li, Q. Wang, and J. He, "Torque calculation of permanent-magnet spherical motor based on permanent-magnet surface current and Lorentz force," *IEEE Trans. Magn.*, vol. 56, no. 5, pp. 1–9, May 2020.

[25] T. L. Tiang, D. Ishak, C. P. Lim, and M. K. M. Jamil, "A comprehensive analytical subdomain model and its field solutions for surface-mounted permanent magnet machines," *IEEE Trans. Magn.*, vol. 51, no. 4, pp. 1–14, Apr. 2015.

[26] Y. Ni, Z. Liu, B. Xiao, and Q. Wang, "Optimum split ratio in surface-mounted permanent magnet machines with pieced Halbach magnet array," *IEEE Trans. Energy Convers.*, vol. 35, no. 4, pp. 1877–1885, Dec. 2020.

[27] P. Liang, F. Chai, Y. Li, and Y. Pei, "Analytical prediction of magnetic field distribution in spoke-type permanent-magnet synchronous machines accounting for bridge saturation and magnet shape," *IEEE Trans. Ind. Electron.*, vol. 64, no. 5, pp. 3479–3488, May 2017.

[28] M. Pourahmadi-Nakhli, A. Rahideh, and M. Mardaneh, "Analytical 2-D model of slotted brushless machines with cubic spoke-type permanent magnets," *IEEE Trans. Energy Convers.*, vol. 33, no. 1, pp. 373–382, Mar. 2018.

[29] Z. Q. Zhu, D. Howe, and C. C. Chan, "Improved analytical model for predicting the magnetic field distribution in brushless permanent-magnet machines," *IEEE Trans. Magn.*, vol. 38, no. 1, pp. 229–238, Jan. 2002.

[30] T. Lubin, S. Mezani, and A. Rezzoug, "Analytical computation of the magnetic field distribution in a magnetic gear," *IEEE Trans. Magn.*, vol. 46, no. 7, pp. 2611–2621, Jul. 2010.

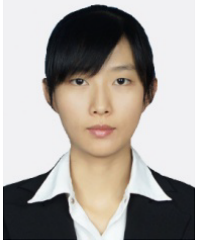

LIANLIAN GAO was born in Yichun, China, in 1990. She received the Ph.D. degree in electrical machine from the Harbin University of Science and Technology, Harbin, China, in 2018.

She is currently a Lecturer with the Harbin University of Science and Technology. Her research interests include research on energy conversion mechanism, analysis and numerical calculation of comprehensive physical field, motor electromagnetic theory, and new technology.

ZHIQIANG CAI was born in Harbin, China, in 1997. He received the B.S. degrees from the Harbin University of Science and Technology, Harbin, in 2019, where he is currently pursuing the M.S. degree in electrical machines.

His research interests include permanent magnet motor electromagnetic theory and design and electromagnetic field calculation.

YANPING LIANG was born in Harbin, China, in 1963. She received the M.S. degree in electrical machine from Harbin University of Science and Technology, Harbin, in 1988, and the Ph.D. degree in electrical machine from the Harbin Institute of Technology, Harbin, in 2005.

She is currently a Professor with the Harbin University of Science and Technology. Her research interests include electrical machine electromagnetic theory and design, large generator electromechanical energy conversion, and electromagnetic field calculation. She is a member of the International Compumag Society (ICS).

DONGMEI WANG was born in Mudanjiang, China, in 1989. She received the B.S. and M.S. degrees from the Harbin University of Science and Technology, Harbin, China, in 2012 and 2015, respectively, where she is currently pursuing the Ph.D. degree in electrical machines. She is also a Lecturer with the Harbin University of Science and Technology. Her current research interests include electromagnetic, fluid, and thermal analysis on electrical machines.

QUN NIU was born in Shandong, China, in 1997. He received the B.S. degree from the Harbin University of Science and Technology, Harbin, China, in 2019. He is currently a Graduate Student with the Harbin University of Science and Technology. His research interests include research on analysis and numerical calculation of comprehensive physical field.

JIA LI was born in Henan, China, in 1997. He is currently pursuing the M.S. degree in electrical machines with the Harbin University of Science and Technology, Harbin, China.

His research interests include analysis of magnetic field and rotor stress of permanent magnet motor.